Draft version August 18, 2015
Preprint typeset using LaTeX style emulateapj v. 5/2/11

DETECTION OF N_2D^+ IN A PROTOPLANETARY DISK

Jane Huang and Karin I. Öberg
Harvard-Smithsonian Center for Astrophysics, 60 Garden St., Cambridge, MA 02138
Draft version August 18, 2015

ABSTRACT

Observations of deuterium fractionation in the solar system, and in interstellar and circumstellar material, are commonly used to constrain the formation environment of volatiles. Toward protoplanetary disks, this approach has been limited by the small number of detected deuterated molecules, i.e. DCO^+ and DCN. Based on ALMA Cycle 2 observations toward the disk around the T Tauri star AS 209, we report the first detection of N_2D^+ (J=3-2) in a protoplanetary disk. These data are used together with previous Submillimeter Array observations of N_2H^+ (J=3-2) to estimate a disk-averaged D/H ratio of 0.3–0.5, an order of magnitude higher than disk-averaged ratios previously derived for DCN/HCN and DCO^+/HCO^+ around other young stars. The high fractionation in N_2H^+ is consistent with model predictions. The presence of abundant N_2D^+ toward AS 209 also suggests that N_2D^+ and the N_2D^+/N_2H^+ ratio can be developed into effective probes of deuterium chemistry, kinematics, and ionization processes outside the CO snowline of disks.

Subject headings: astrochemistry—ISM: molecules—protoplanetary disks

1. INTRODUCTION

The gas and dust disks surrounding young stars are the formation sites of planets. Obtaining a chemical inventory of these disks is key to developing effective molecular probes of disk ionization, temperature, and other characteristics that set planet formation efficiencies. Applying such probes to disk studies can illuminate the processes that led to the present-day composition of solar system bodies and exoplanets.

The thermal histories of solar system, protoplanetary disk and interstellar material are often probed via measurements of deuterated isotopologues of common molecules (e.g. Aikawa & Herbst 1999; Mumma & Charnley 2011). Molecular D/H ratios in cold interstellar and circumstellar environments can be several orders of magnitude greater than the cosmic D/H abundance of $\sim 10^{-5}$ (e.g., Crapsi et al. 2005; Qi et al. 2008; Öberg et al. 2012; Teague et al. 2015). The increase in the D/H ratio of specific molecules, i.e. the deuterium fractionation, is a consequence of the lower zero-point energies of deuterated molecules compared to their non-deuterated isotopologues. The resulting small energy barrier for a molecule to exchange a deuterium atom for a hydrogen atom favors deuterium fractionation in cold environments. High D/H ratios in the ISM help to identify regions that are currently cold, e.g. pre-stellar cores, and to infer a low-temperature history for material in warmer regions. In the solar system, measurements of D/H ratios in comets set constraints upon the temperature (and therefore the location) at which they formed in the Solar nebula (e.g. Hartogh et al. 2011; Altwegg et al. 2015), and the high D/H ratio of terrestrial water indicates inheritance from the cold parent molecular cloud (Cleeves et al. 2014b).

Although more than 30 deuterated molecules have been detected throughout various pre-stellar and protostellar environments (see Roueff & Gerin 2003, Ceccarelli et al. 2007 and references therein), only two of them, DCO^+ and DCN, had been detected in protoplanetary disks (van Dishoeck et al. 2003; Qi et al. 2008). A third deuterated molecule that has been predicted to be abundant in disks is N_2D^+ (Willacy 2007). N_2D^+ forms via the reaction (Dalgarno & Lepp 1984)

$$H_2D^+ + N_2 \rightarrow H_2 + N_2D^+. \quad (1)$$

The formation of H_2D^+ compared to H_3^+ is enhanced at temperatures below 50 K (Herbst 1982; Ceccarelli et al. 2014). This leads to an increase in the N_2D^+/N_2H^+ ratio in cold environments. Because H_2D^+ is efficiently destroyed by gas-phase CO, abundant N_2D^+, co-existing with its non-deuterated isotopologue N_2H^+, is only expected outside the CO snowline, where CO freezes out on grains (Qi et al. 2013b). Together with N_2H^+, N_2D^+ may be the best and perhaps only tracer of the chemistry and ionization of the midplane in the outer disk region (Cleeves et al. 2014a), the proposed formation site of Kuiper Belt objects, comets, Uranus, and Neptune (Qi et al. 2013b; Ali-Dib et al. 2014).

As part of an ALMA Cycle 2 disk survey of deuterated molecules, we searched for N_2D^+ toward AS 209, a 1.6 Myr old K5 T Tauri star in ρ Ophiuchi located 130± 50 pc away (Herbig & Bell 1988; van Leeuwen 2007). AS 209 is surrounded by a large and gas-rich disk, extending out to 340 AU in CO emission (Andrews et al. 2009; Öberg et al. 2011). Molecules previously detected in the disk include CO, HCO^+, DCO^+, N_2H^+, HCN, and CN (Öberg et al. 2011). In this letter, we present the first detection of N_2D^+ in a protoplanetary disk. We use existing Submillimeter Array observations of N_2H^+ in the same disk to calculate its deuterium fractionation and discuss the implications for future disk studies.

2. OBSERVATIONS

AS 209 (J2000.0 R.A. $16^h49^m15^s.29$, decl. $-14°22'08''.6$) was observed 2014 July 2 during ALMA Cycle 2 with 21 minutes of on-source integration time. Thirty-four 12 m antennae were used for the observations, with a maximum baseline of 650.3 m.

Thirteen spectral windows (SPWs) were observed in Band 6, each with 61.04 kHz resolution. The N_2D^+ J=3-2 line was in SPW 9, centered on 231.32183 GHz, and the ^{13}CO J=2-1 line (used in this study as a v_{LSR} and spectral profile reference) was in SPW 7, centered on 220.39868 GHz. The 1.4 mm dust continuum flux was extracted by averaging the channels in five line-free SPWs. Each of these windows was 59 MHz wide.

ALMA/NAASC staff performed bandpass and phase calibration with the quasar J1733-1304, and the flux was calibrated with Titan. The uncertainty in the absolute flux is ∼10%. The calibrated visibilities were deconvolved and CLEANed with the CASA software package (version 4.2.2). The integrated flux density of the 1.4 mm dust continuum is 242±24 mJy. This was measured by integrating over the area of the disk delimited by a 2σ contour, where σ=0.3 mJy beam^{-1} was the continuum rms measured in a signal-free region of the intensity map. After continuum subtraction in the uv-plane, the data cubes for the SPWs were rebinned to 0.4 km/s. To increase signal to noise, the visibilities for the N_2D^+ J=3-2 line were tapered to 1″. Because the spatial distribution of the emission changes between different velocity channels, CLEANing for both N_2D^+ and ^{13}CO was performed using a Keplerian rotation mask based on the emission patterns of the stronger line, ^{13}CO 2-1. The channel rms for ^{13}CO 2-1 was 17 mJy beam^{-1}, while the rms for N_2D^+ 3-2 was 8.5 mJy beam^{-1}.

To estimate a D/H ratio for N_2D^+/ N_2H^+, this paper also uses AS 209 data originally published in Öberg et al.'s Submillimeter Array protoplanetary disk survey (2011). The 1.4 mm dust continuum flux density from their dataset (also obtained by integrating over the area of the disk encompassed by the 2σ contour) is 219 ± 22 mJy. Thus, within the uncertainties, the flux density from the ALMA observations is consistent with that of the SMA observations.

3. RESULTS

Figure 1 shows the AS 209 1.4 mm dust continuum, integrated intensity maps (spanning channels from 2.6 to 7.0 km s^{-1}), and blue and redshifted disk emission maps for the N_2D^+ 3-2 and ^{13}CO 2-1 lines. The CO emission is symmetric, whereas most of the emission above the 2σ level for N_2D^+ 3-2 is east of the phase center. The peak intensity of N_2D^+ is 3.3σ, where σ=12 mJy beam^{-1} km s^{-1} is the rms measured in a signal-free portion of the integrated intensity map. The velocity field of ^{13}CO 2-1 in Fig. 1 is well-resolved and consistent with the Keplerian rotation of a disk. The redshifted N_2D^+ emission is consistent with the redshifted ^{13}CO emission, but no blueshifted emission is observed for N_2D^+ above the 2σ level. This is spatially consistent with the asymmetry observed in the total integrated intensity map. While the morphologies of the contours differ between the total integrated intensity maps and the redshifted emission maps for N_2D^+ due to the differing noise contributions for the different velocity ranges, the mean intensity measured from the integrated intensity map is within 5% of the mean intensity measured over the redshifted channels only, confirming that most of the emission is redshifted.

Velocity channel maps for N_2D^+ 3-2 are shown in Fig. 2. Line flux at >3σ level is detected near the phase center

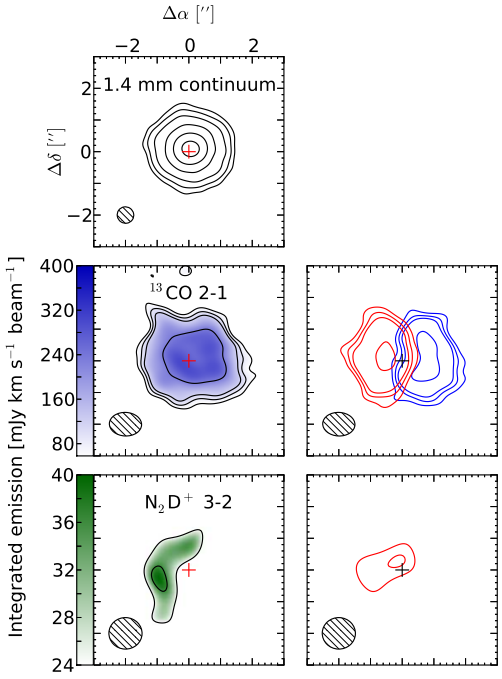

Figure 1. Continuum and line emission maps toward AS 209. The topmost panel shows the 1.4 mm dust continuum emission, with contours at [5, 10, 20, 40, 80, 160]σ, where σ = 0.3 mJy beam^{-1}. Integrated intensity maps (summed from 2.6 to 7.0 km s^{-1}) with contours at [2, 3, 4, 8]σ are shown in the left column for ^{13}CO 2-1 , with σ = 29 mJy km s^{-1} beam^{-1}, and N_2D^+ 3-2, with σ = 12 mJy km s^{-1} beam^{-1}. The corresponding panels in the right column show the integrated intensities for the blueshifted (2.6 to 4.6 km s^{-1}) and redshifted (5.0 to 7.0 km s^{-1}) emission. The pointing center in each panel is marked by a cross, with position offsets in arcseconds. Synthesized beams are drawn in the lower left of each panel.

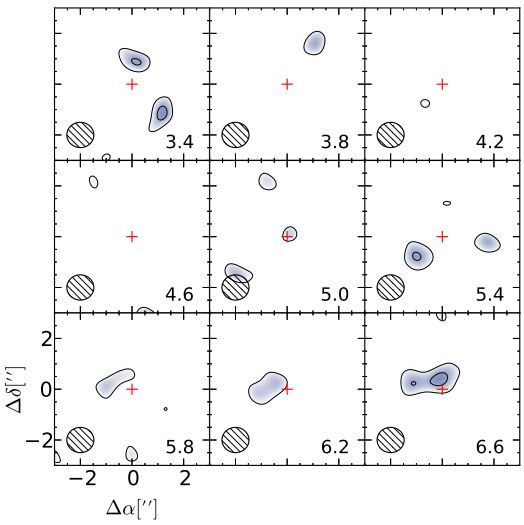

Figure 2. Velocity channel maps of N_2D^+ 3-2 emission toward AS 209, binned by 0.4 km s^{-1}. 2σ and 3σ contours are drawn, with σ = 8.5 mJy beam^{-1}. Channel velocities [km s^{-1}] are listed in the lower right corner of each panel. The pointing center is denoted by a cross, with offsets from the pointing center indicated in arcseconds on the axes. Synthesized beams are drawn in the lower left of each panel.

in three channels, and at the 2σ level in another three channels. The progression of emission from west to east of the pointing center is consistent with disk rotation, confirming the disk origin of the N_2D^+ emission shown in Fig. 1. We note that although blueshifted emission is visible in the velocity channel maps, it is not apparent in the integrated intensity map in Fig. 1 above the 2σ level because the map is integrated across a velocity range that includes a number of channels without blueshifted emission.

Figure 3 displays spectra for the N_2D^+ 3-2 and ^{13}CO 2-1 lines, extracted using the Keplerian CLEAN masks, together with the N_2H^+ 3-2 SMA spectrum. The double-peaked profile of ^{13}CO 2-1 is typical of a rotating disk. The spectrum of N_2H^+ 3-2, though with a lower signal-to-noise ratio (SNR), is also consistent with a double-peaked profile. As with the integrated intensity maps, the emission for N_2D^+ is asymmetric, with only the red-shifted peak clearly visible. However, the position of the N_2D^+ peak is consistent with the positions of the red-shifted peaks for N_2H^+ and ^{13}CO. The hyperfine structure is not resolved for N_2D^+.

The integrated fluxes are given in Table 1. The uncertainty on the integrated flux was calculated using the formula $\sigma = \mathrm{rms} \times \mathrm{FWHM}/\sqrt{n_{ch}}$, where the rms is measured from a featureless portion of the spectrum for each transition, the FWHM is measured from the ^{13}CO 2-1 line, and n_{ch} is the number of channels spanning the FWHM.

Using the N_2H^+ line data from Öberg et al. (2011) in conjunction with the ALMA observations of N_2D^+, we estimate a disk-averaged N_2D^+/N_2H^+ ratio toward AS 209. Because the SNR is low for both molecules, their spatial distributions are not well-constrained by the current set of observations. Hence we assume that the molecules are co-spatial in the disk based on their similar formation and destruction chemistry. In particular, the N_2D^+ and N_2H^+ distributions are both expected to be regulated by destructive reactions with CO gas, and therefore the degree of freeze-out of CO and N_2. The N_2H^+ intensity, averaged over a $5'' \times 5''$ circle centered on the continuum peak, is 320 ± 40 mJy beam^{-1} km s^{-1}, while the N_2D^+ intensity, averaged over a $4'' \times 4''$ circle centered on the continuum peak, is 9 ± 2 mJy beam^{-1} km s^{-1}. In each case, the surface area over which the intensity was averaged was based on the extent of the molecular emission above the $2\times$rms level and was largely set by the synthesized beam size.

Column densities were derived from the integrated intensities using the LTE formula from Remijan et al. (2003), in the case where the emission is optically thin and the continuum brightness temperature is assumed to be much lower than the excitation temperature:

$$N = \frac{2.04 \int \Delta I \; dv}{\theta_a \theta_b} \frac{Q_{rot} e^{E_u/T_e}}{\nu^3 \langle S_{ij} \mu^2 \rangle} \times 10^{20} \text{ cm}^{-2}. \quad (2)$$

$\int \Delta I \; dv$ (Jy beam^{-1} km s^{-1}) is the integrated line intensity, θ_a and θ_b (arcsec) are the major and minor axes of the ellipse defined by the FWHM of the Gaussian beam, and T_e (K) is the excitation temperature. The molecular parameters, which are the rotational partition function Q_{rot}, transition upper state energy E_u (K), transition rest frequency ν (GHz), line strength S, and electric dipole moment μ (Debye), were all obtained from the Cologne Database for Molecular Spectroscopy (Müller et al. 2001, 2005).

The excitation temperature is expected to be between 10 and 25 K in the outer regions of the disk where N_2D^+ and N_2H^+ reside (e.g. Willacy 2007; Ceccarelli et al. 2014). At 10 K, the disk-averaged column density of N_2D^+ is $2.1 \pm 0.5 \times 10^{11}$ cm^{-2} and that of N_2H^+ is $6.3 \pm 0.8 \times 10^{11}$ cm^{-2}. At 25 K, the disk-averaged column density of N_2D^+ is $1.4 \pm 0.3 \times 10^{11}$ cm^{-2} and that of N_2H^+ is $3.1 \pm 0.4 \times 10^{11}$ cm^{-2}. At a given temperature, the dominant source of uncertainty in the LTE approximation for the column density is due to the uncertainty on the intensity measurement. The resulting D/H ratio is estimated to be between 0.3 and 0.5. As long as the N_2D^+ and N_2H^+ are co-spatial, the ratios of their disk-averaged column densities can be estimated with greater confidence than their absolute column densities, which are more sensitive to the assumed surface area of the emission.

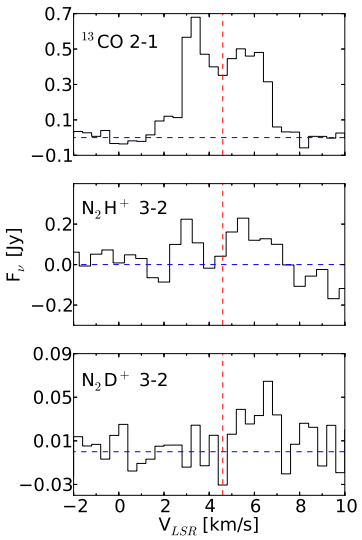

Figure 3. Spectra of the ^{13}CO 2-1 and N_2D^+ 3-2 transitions (extracted with Keplerian masks) toward AS 209, as well as a spectrum of N_2H^+ 3-2 toward AS 209 from Submillimeter Array data published in Öberg et al. (2011). The v_{LSR} is marked by the vertical dashed lines.

To check the validity of the optically thin LTE approximation for estimating the column densities of N_2H^+ and N_2D^+ toward AS 209, column densities for N_2H^+ were also calculated with RADEX, a 1D non-LTE radiative transfer code (van der Tak et al. 2007). To cover the range of typical disk conditions, we ran a grid of models with kinetic temperatures between 10 and 25 K and an H_2 number density (representing the dominant collision partner) of 10^6–10^{10} cm^{-3}. The resulting column densities ranged from 1.7 to 7.8×10^{11} cm^{-2}, similar to the column density range estimated through LTE calculations.

4. DISCUSSION

4.1. *N_2H^+ deuterium fractionation*

Table 1
Summary of Line Observations

Transition	Rest Frequency (GHz)	E_u (K)	Beam	Integrated Flux (mJy km s^{-1})	Channel rms (mJy $beam^{-1}$)
^{13}CO J=2-1[a]	220.39868	15.9	1.″02× 0.″74 (87°.18)	1940[37]	17
N_2D^+ J=3-2[a]	231.32183	22.2	1.″05× 0.″99 (87°.83)	80[18]	8.5
N_2H^+ J=3-2[b]	279.51173	26.8	3.″74× 2.″50 (19°.26)	597[78]	80

[a] From ALMA observations.
[b] From data originally published in Öberg et al. (2011).

The estimated N_2D^+/N_2H^+ disk-averaged abundance ratio of 0.3-0.5 is consistent with the disk models of Willacy (2007), in which the D/H ratio was predicted to range between 0.35 and 7.0 in the outer disk. The predicted range reflects the dependence of deuterium chemistry on desorption from dust grains due to cosmic rays, thermal processes, and UV radiation, which varied between models. Willacy (2007) also predicted that the D/H ratio for N_2D^+ in the outer disk would be one or two orders of magnitude greater than the corresponding ratios for DCN and DCO^+. This is consistent with our finding that the disk-averaged D/H ratio for N_2H^+ toward AS 209 is at least an order of magnitude higher than the disk-averaged ratios derived for HCN and HCO^+ toward other disks. A disk-averaged DCN/HCN abundance ratio of 0.017 was derived for TW Hya (Öberg et al. 2012). Disk-averaged DCO^+/HCO^+ abundance ratios have been estimated to be 4×10^{-3} toward DM Tau, 0.02 toward HD 163296, and 0.035 toward TW Hya (van Dishoeck et al. 2003; Guilloteau et al. 2006; Mathews et al. 2013). However, analyses of spatially resolved data for these three disks have found local DCO^+/HCO^+ ratios rising as high as 0.1-0.3, with radial variations in the abundances due to radial changes in the temperature (Qi et al. 2008; Mathews et al. 2013; Teague et al. 2015). The local enhancement levels revealed by the spatially resolved data indicates the value of obtaining spatially resolved data for other deuterated lines, such as N_2D^+.

The high D/H ratio for N_2D^+/N_2H^+ toward AS 209 and the lower DCO^+/HCO^+ ratios found in other protoplanetary disks suggest that the deuterium chemistry in the outer disk resembles that of dense cores and protostellar envelopes. A survey of low-mass starless cores found N_2D^+/N_2H^+ ratios ranging from <.02 to .44 (Crapsi et al. 2005), and a survey of Class 0 protostars found N_2D^+/N_2H^+ ratios ranging from <.034 to .27 (Emprechtinger et al. 2009). For the Class 0 protostars in which both N_2D^+ and DCO^+ have been measured, the N_2D^+/N_2H^+ ratio often exceeds the DCO^+/HCO^+ ratio by an order of magnitude (Jørgensen et al. 2004; Emprechtinger et al. 2009). Similarly, toward the dense core L1544, Caselli et al. (2002b) found that N_2D^+/N_2H^+ was ∼0.2, versus a ratio of 0.04 for DCO^+/HCO^+.

Given that models posit similar formation pathways for N_2D^+ and DCO^+, it may be surprising that such different D/H ratios are predicted and observed for the two molecules. This difference arises because gas-phase CO, a parent molecule of DCO^+, destroys H_2D^+, one of the main parent molecules of N_2H^+ and N_2D^+ (Qi et al. 2013a). Due to this destruction pathway, N_2D^+ is only abundant at low temperatures, where deuterium fractionation is especially efficient and gas-phase CO is depleted due to freezeout onto grains.

4.2. *N_2D^+ emission asymmetry*

The N_2D^+ emission toward AS 209 appears to be asymmetric. Higher SNR observations are required to confirm the reality of this asymmetry, but it is worth considering possible causes for this tentative azimuthal N_2D^+ variation. Previously observed azimuthal variations in disk molecular emission have been ascribed to foreground absorption, projection effects due to disk inclination, and dust traps cooling nearby gas (e.g. Öberg et al. 2011; Rosenfeld et al. 2013; van der Plas et al. 2014). Foreground absorption is unlikely to cause asymmetric emission for N_2D^+ due to the molecule's low abundance and high critical density. For molecular emission originating close to the cold midplane, as is expected for N_2D^+, projection effects should also play a minimal role (Rosenfeld et al. 2013). Asymmetry in the dust structure is an unlikely cause, given the axisymmetric appearance of the 1.4 mm continuum emission shown in Fig. 1. However, because the N_2D^+ distribution is expected to be especially sensitive to ionization and temperature, possible causes for asymmetry include X-ray flares or azimuthal density gradients in the outer disk (e.g. Birnstiel et al. 2013; Cleeves et al. 2015). Temperature asymmetries could be probed with D/H ratios derived from high SNR spatially-resolved observations of N_2D^+ and N_2H^+, while asymmetry in the midplane ionization structure could be evaluated by comparing N_2D^+ to neutral tracers such as H_2CO, another molecule expected to form past the CO snowline (Qi et al. 2013a).

4.3. *Developing N_2D^+ as a disk probe*

The similarity between the deuterium fractionation in disks and interstellar cloud cores suggest that analogous to its use as a tracer of CO-depleted cold gas in cores (Caselli et al. 2002a; Emprechtinger et al. 2009), N_2D^+ with N_2H^+ could be developed into a unique tracer of the cold, CO-depleted outer disk midplane. In addition, measurements of N_2D^+ and N_2H^+, together with DCO^+ and HCO^+, have been used to estimate the ionization fraction of cloud cores (Caselli et al. 1998, 2002b). This approach could be adapted to evaluate the ionization fraction of disks.

Spatially resolved observations through ALMA would allow the D/H ratio as a function of radius to be derived, thereby providing a stronger test for chemical theories regarding how N_2D^+ is formed and destroyed throughout

disks. A sensitive survey of N_2D^+ and N_2H^+ in disks would also be useful to determine the relationship between deuterium fractionation and other properties of the disk, such as mass, age, and ionization processes.

As molecules with abundances anti-correlated with the abundances of CO isotopologues and related species (e.g. HCO^+, DCO^+), N_2D^+ and N_2H^+ complement the current set of common disk tracers. While previously detected disk molecules have been abundant in the inner disk and in the warm molecular layer high above the midplane, N_2D^+ and N_2H^+ are suitable for tracing kinematics, ionization, and temperature structure in the outer disk midplane. Although H_2D^+ is also expected to be abundant in the outer disk midplane, it has not yet been detected in disks and is expected to require very long integration (Cleeves et al. 2014a). Therefore, further observations and modeling of N_2D^+ and N_2H^+ are key to developing a fuller picture of how disk characteristics vary spatially. Constraining such properties can clarify how volatiles have been formed, transported, or destroyed in disks, giving rise to the planets we observe now.

This paper makes use of the following ALMA data: ADS/JAO.ALMA#2013.1.00226. ALMA is a partnership of ESO (representing its member states), NSF (USA) and NINS (Japan), together with NRC (Canada) and NSC and ASIAA (Taiwan), in cooperation with the Republic of Chile. The Joint ALMA Observatory is operated by ESO, AUI/NRAO and NAOJ. The National Radio Astronomy Observatory is a facility of the National Science Foundation operated under cooperative agreement by Associated Universities, Inc. We thank Adam Leroy and the NAASC for assistance with calibration and imaging, Ryan Loomis and Viviana Guzman for helpful discussions on the data, and the referee for useful comments on the paper. K. I. O. also acknowledges funding from the Simons Collaboration on the Origins of Life (SCOL), the Alfred P. Sloan Foundation, and the David and Lucile Packard Foundation.

REFERENCES

Aikawa, Y., & Herbst, E. 1999, ApJ, 526, 314
Ali-Dib, M., Mousis, O., Petit, J.-M., & Lunine, J. I. 2014, ApJ, 793, 9
Altwegg, K., Balsiger, H., Bar-Nun, A., et al. 2015, Science, 347, A387
Andrews, S. M., Wilner, D. J., Hughes, A. M., Qi, C., & Dullemond, C. P. 2009, ApJ, 700, 1502
Birnstiel, T., Dullemond, C. P.,& Pinilla, P. 2013, A&A, 550, L8
Caselli, P., Walmsley, C. M., Terzieva, R., et al. 1998, ApJ, 499, 234
Caselli, P., Walmsley, C. M., Zucconi, A., et al. 2002a, ApJ, 565, 331
Caselli, P., Walmsley, C. M., Zucconi, A., et al. 2002b, ApJ, 565, 344
Ceccarelli, C., Caselli, P., Bockelée-Morvan, D., et al. 2014, Protostars and Planets VI, 859
Ceccarelli, C., Caselli, P., Herbst, E., Tielens, A. G. G. M., & Caux, E. 2007, Protostars and Planets V, 47
Cleeves, L. I., Bergin, E. A., & Adams, F. C. 2014a, ApJ, 794, 123
Cleeves, L. I., Bergin, E. A., Alexander, C. M. O. ., et al. 2014b, Science, 345, 1590
Cleeves, L. I., Bergin, E. A., Qi, C., Adams, F. C. & Öberg, K. I. 2015, ApJ, 799, 204
Crapsi, A., Caselli, P., Walmsley, C. M., et al. 2005, ApJ, 619, 379
Dalgarno, A., & Lepp, S. 1984, ApJ, 287, L47
Emprechtinger, M., Caselli, P., Volgenau, N. H., Stutzki, J., & Wiedner, M. C. 2009, A&A, 493, 89
Guilloteau, S., Piétu, V., Dutrey, A., & Guélin, M. 2006, A&A, 448, L5
Hartogh, P., Lis, D. C., Bockelée-Morvan, D., et al. 2011, Nature, 478, 218
Herbig, G. H., & Bell, K. R. 1988, Third Catalog of Emission-Line Stars of the Orion Population : 3 : 1988
Herbst, E. 1982, A&A, 111, 76
Jørgensen, J. K., Schöier, F. L., & van Dishoeck, E. F. 2004, A&A, 416, 603
Müller, H. S. P., Schlöder, F., Stutzki, J., & Winnewisser, G. 2005, Journal of Molecular Structure, 742, 215
Müller, H. S. P., Thorwirth, S., Roth, D. A., & Winnewisser, G. 2001, A&A, 370, L49
Mathews, G. S., Klaassen, P. D., Juhász, A., et al. 2013, A&A, 557, 132
Mumma, M. J., & Charnley, S. B. 2011, ARA&A, 49, 471
Öberg, K. I., Qi, C., Fogel, J. K. J., et al. 2011, ApJ, 734, 98
Öberg, K. I., Qi, C., Wilner, D. J., & Hogerheijde, M. R. 2012, ApJ, 749, 162
Qi, C., Öberg, K. I., & Wilner, D. J. 2013a, ApJ, 765, 34
Qi, C., Öberg, K. I., Wilner, D. J., et al. 2013b, Science, 341, 630
Qi, C., Wilner, D. J., Aikawa, Y., Blake, G. A., & Hogerheijde, M. R. 2008, ApJ, 681, 1396
Remijan, A., Snyder, L. E., Friedel, D. N., Liu, S.-Y., & Shah, R. Y. 2003, ApJ, 590, 314
Rosenfeld, K. A., Andrews, S. M., Hughes, A. M., Wilner, D. J., & Qi, C. 2013, ApJ, 774, 16
Roueff, E., & Gerin, M. 2003, Space Sci. Rev., 106, 61
Teague, R., Semenov, D., Guilloteau, S., et al. 2015, A&A, 574, A137
van der Plas, G., Casassus, S., Ménard, F., et al. 2014, ApJ, 792, L25
van der Tak, F. F. S., Black, J. H., Schöier, F. L., Jansen, D. J., & van Dishoeck, E. F. 2007, A&A, 468, 627
van Dishoeck, E. F., Thi, W.-F., & van Zadelhoff, G.-J. 2003, A&A, 400, L1
van Leeuwen, F. 2007, A&A, 474, 653
Willacy, K. 2007, ApJ, 660, 441